DII-7 TRANSIENT ANALYSIS IN A FRACTURING EPOXY PLATE WITH A CENTRAL NOTCH

A. S. Kobayashi*, W. B. Bradley** and R. A. Selby***

## ABSTRACT

Transient displacement distributions in fracturing epoxy plates were determined experimentally in centrally notched epoxy plates by the Moire fringe method. Transient Moire fringe patterns were either scanned by a microdensitometer for accurate determination of the locations of fractional fringes or Westergaard's stress functions were fitted to data points obtained by direct measurements. In most cases, the displacement distributions in the vicinity of the running crack tips varied as $\sqrt{r}$. Distributions of normal strains in the longitudinal direction, of principal strains, and of maximum shear strains were determined for various crack tip locations in the plates.

## INTRODUCTION

Since the pioneering work of Wells and Post (1,2)****, experimental efforts in the area of the transient analysis of displacement, strain and stress fields associated with brittle fracture have been lagging. Papers by Rolfe and Hall (3) and by Cargill (4) reported strain-time results obtained by strain gage method in fracturing steel plates. Due to limited instrumentation these results do not yield complete information on the characteristics of the stress fields surrounding the running crack tip.

The general objective of this paper is to present some preliminary results on the transient states of displacements and strains in the vicinity of a running crack tip. Specifically, this paper investigates the possibility of extending the static Griffith-Irwin theory of fracture mechanics to the dynamic problem of a running crack. This possible extension was

---

* Associate Professor, Department of Mechanical Engineering, University of Washington, Seattle, Washington

** Research Associate, Department of Mechanical Engineering, University of Washington, Seattle, Washington

*** Engineer, Sandia Corporation, Livermore, California

**** Numbers in parenthesis refer to references at the end.

motivated by the theoretical solutions for running cracks by Yoffe (5), Baker (6), and Craggs (7) where these investigators concluded that the $1/\sqrt{r}$ singularity was preserved from equivalent static analysis.

In selecting a suitable experimental technique for this investigation, a method of whole-field strain determination was deemed important since the running crack tends to branch or curve when reaching a terminal velocity. The photoelastic method of Wells and Post (1) was not used because the stress optical coefficient of the material depends on the particle velocity which varies throughout the specimen at any instant of time, thus posing a problem of converting the photoelastic fringes into stresses or strains.

The experimental technique used for this investigation was the Moire fringe method (see for example references 8,9) and its application to transient strain analysis is not new (10). With the present state of the art, however, the method when applied to common structural materials suffers from lack of sensitivity in determining elastic strains unless partial fringe orders are measured and numerical data processing techniques are used (11). Such procedures were not available to the authors and therefore a combination of experimental and numerical procedures was developed for evaluating the massive amount of data necessary for determining the elastic strain field in the vicinity of the running crack tip.

## THEORETICAL BACKGROUND

The state of stresses in front of a static crack can be conveniently represented by Westergaard's stress function, Z, in a complex domain z, as shown in Figure 1, as (12),

$$\sigma_{xx} = \text{Re } Z - y \text{ Im } Z'$$

$$\sigma_{yy} = \text{Re } Z + y \text{ Im } Z' \qquad (1)$$

$$\sigma_{xy} = -y \text{ Re } Z'$$

where $Z' = \frac{dZ}{dz}$.

Furthermore for a symmetrical loading about the x and y axes in a finite plate, the complex stress function, Z, can be approximated by a polynomial in z with only real coefficients of $C_{2m+1}$ as

$$Z = \sum_{m=0}^{m=n} \frac{C_{2m+1} z^{2m+1}}{\sqrt{z^2 - a^2}} \qquad (2)$$

where $z = \pm a$ is the location of the two crack tips on the x-axis.





For the case of a moving Griffith crack, the state of stresses was represented by Yoffe with this form of Westergaard's stress function by considering a constant length crack moving at a constant velocity (5). The coefficients, $C_{2m+1}$, are now a function of the crack velocity and of the velocities of longitudinal and shear waves in addition to the boundary conditions and the dynamic properties of the material. Although this theoretical simulation of the actual running crack by the Yoffe type of moving Griffith crack is in error, it is considered a good approximation when the crack velocity is substantially lower than the velocities of the stress waves (13, 14) since at low crack velocity, the state of stresses in the vicinity of the running crack tip will have essentially the characteristics of the static crack.

The Moire fringe method determines the displacement field directly, and therefore the stress function, Z, was determined by fitting this function to the experimentally determined displacement field in the vicinity of the running crack tip. These displacement components in plane stress can be represented as

$$u = \frac{1}{G}\left[\frac{1-\nu}{2(1+\nu)} \text{Re } \bar{Z} - \frac{y}{2} \text{Im } Z\right]$$

$$v = \frac{1}{G}\left[\frac{1}{1+\nu} \text{Im } \bar{Z} - \frac{y}{2} \text{Re } Z\right] \qquad (3)$$

where $Z = \frac{d\bar{Z}}{dz}$

G is the shear modulus and $\nu$ is the Poisson's ratio of the material. In actual computation, however, the term $\frac{1}{G}$ in Equation 3 was combined with the undetermined coefficients $C_{2m+1}$ such that the redefined coefficient, $\underline{C}_{2m+1}$, contained the shear modulus as

$$\underline{C}_{2m+1} = \frac{C_{2m+1}}{G} \qquad (4)$$

Having determined the coefficients of the stress function from the experimentally measured displacement field, the state of stresses can thus be computed by Equation 1. In actual computation, however, the state of stresses was not determined since it depends upon the value of the dynamic shear modulus which, for the material used in this investigation, was somewhat strain rate sensitive. Instead, the state of strains which does not require the knowledge of dynamic shear modulus was computed. The strain components in terms of Westergaard's stress function are

$$\varepsilon_{xx} = \left[\frac{1-\nu}{2(1+\nu)} \text{Re } \left(\frac{Z}{G}\right) - \frac{y}{2} \text{Im } \left(\frac{Z'}{G}\right)\right]$$

$$\varepsilon_{yy} = \left[\frac{1-\nu}{2(1+\nu)} \text{Re } \left(\frac{Z}{G}\right) + \frac{y}{2} \text{Im } \left(\frac{Z'}{G}\right)\right] \qquad (5)$$

$$\varepsilon_{xy} = \frac{-\gamma}{2} \text{Re} \left(\frac{Z'}{G}\right)$$

It should be noted that Equation 4 contains the Poisson's ratio which was assumed to remain constant for this material. Also an inspection of Equations 3 and 5 shows that by redefining the undetermined coefficient as $C_{2m+1}$, it is now possible to determine the strains directly from Westergaard's stress function without using the dynamic shear modulus.

Finally, from linear fracture mechanics the stress intensity factor K and the crack extension force $\mathcal{G}$ for the state of plane stress can be represented as

$$\frac{K}{G} = \frac{\pi}{a} \sum_{m=0}^{m=n} C_{2m+1} a^{2m+1} \qquad (6)$$

and for the state of plane stress

$$\mathcal{G} = \frac{K^2}{E} \qquad (7)$$

For the state of stresses in the immediate vicinity of the crack tip, then Equations 1 and 3 can be expressed in terms of the local coordinates, r and θ, shown in Figure 1, as

$$\sigma_{xx} = \frac{K}{\sqrt{2\pi r}} \cos\frac{\theta}{2} \left[1 - \sin\frac{\theta}{2} \sin\frac{3\theta}{2}\right]$$

$$\sigma_{yy} = \frac{K}{\sqrt{2\pi r}} \cos\frac{\theta}{2} \left[1 + \sin\frac{\theta}{2} \sin\frac{3\theta}{2}\right] \qquad (8)$$

$$\sigma_{xy} = \frac{K}{\sqrt{2\pi r}} \sin\frac{\theta}{2} \cos\frac{\theta}{2} \cos\frac{3\theta}{2}$$

where Westergaard's stress function becomes

$$Z = \frac{K}{\sqrt{2\pi r}} e^{-i\frac{\theta}{2}}$$

and

$$\bar{Z} = \sqrt{\frac{2r}{\pi}} K e^{i\frac{\theta}{2}}$$

and the displacement components for the case of plane stress are





$$u = \frac{K}{G} \sqrt{\frac{r}{2\pi}} \cos\frac{\theta}{2} \left[\frac{1-\nu}{1+\nu} + \sin^2\frac{\theta}{2}\right]$$

$$v = \frac{K}{G} \sqrt{\frac{r}{2\pi}} \sin\frac{\theta}{2} \left[\frac{2}{1+\nu} - \cos^2\frac{\theta}{2}\right] \qquad (9)$$

From the measured value of u or v in the vicinity of the crack tip, one can determine the approximate dynamic stress intensity factor by Equation 9. These approximate stress intensity factors may be compared with the more exact results obtained by the use of Equation 6.

## EXPERIMENTAL PROCEDURE

The specimens were a 4-in. wide and approximately 0.2-in. thick epoxy plate with central cracks of initial crack lengths varying from 0.2 to 1.0 inch as shown in Figure 2. A rectangular array of 1,000 dots-per-linear-inch pattern was photo-printed on each specimen either in directions parallel and perpendicular or 45° to the crack. By attaching a line master grid of approximately 992 lines per inch parallel to the direction of the dot pattern on the specimen, a residual Moire fringe pattern was formed as shown in later figures. This procedure, commonly referred to as the mismatch technique in the Moire fringe method, increases the sensitivity of the displacement determination.

The specimen was then loaded in a fracture test stand with the associated instrumentation shown schematically in Figure 3. Upon the inception of fracture, the running crack propagated through the conducting paint which triggered a microflash unit and recorded a single photograph of the transient Moire fringe pattern. This high speed photographic system is shown schematically in Figure 4. Twelve test results recorded by this experimental procedure are reported in this paper.

## TRANSIENT MOIRE FRINGE PATTERNS

Typical Moire fringe patterns are shown in Figures 5 through 7. The line master grids and photo-printed dot patterns in Figures 5 and 7 were perpendicular and parallel to the crack, while in Figure 6 they were placed at 45° to the crack. Table I shows the orientation of the fringes for each specimen. Also shown in Table I are the calculated static fracture toughness values of the material, $K_{sc} = \sqrt{\pi}\,\sigma\,\sqrt{a}$, wherever it was possible to determine. An average fracture toughness of 305 psi $\sqrt{\text{in.}}$, thus determined, was used to determine the ratios of the dynamic stress intensity factors to the static fracture toughness. As an example of unusual cracks, Figure 7a shows an enlargement of a crack which started at two locations due to a defective initial crack tip. These two cracks subsequently joined together

and ran as a single crack. In Figure 7b, the initial stage of the branching of a crack can be seen in both tips of the crack. The mismatch in this particular specimen was increased to approximately 35 Moire fringes per inch. Two specimens with such increased mismatch, specimens K and L, were tested in order to obtain displacement measurements closer to the tips of the running crack. These Moire fringes in Figure 7b are curved in opposite directions in comparison with the Moire fringes in other figures due to compressive mismatch between the lined master and the dot pattern on the specimen. All other mismatches were tensile in direction.

## EVALUATION OF EXPERIMENTAL RESULTS

From the transient Moire fringe patterns, displacements were determined along a line which passed through the crack tip perpendicular to the direction of the unloaded Moire line and dot grids. These displacements were plotted against the distance, r, from the crack tip on a log-log scale. A typical plot of this displacement is shown in Figure 8. The mismatch in this specimen was 35 Moire fringes per inch and therefore data points as close as r = 0.02" from the crack tip were obtained. Other plots include data points as close as r = 0.1" from the crack tip. Moire fringe patterns corresponding to x-displacements, u, were not evaluated due to the small magnitudes of displacements obtained. All other patterns with the exception of the double and branched cracks were evaluated.

The slopes adjacent to the crack tip of these displacement curves were then measured for every specimen. As shown in Table III, these slopes were approximately equal to 1/2, within $\pm 12\%$, which substantiates the initial assumption that the characteristic of a static crack will prevail in the vicinity of a running crack in a brittle material as long as the crack velocity is low compared to the shear wave velocity. Exception to this postulate can be seen in the case of the double and branching cracks shown in Figure 7 and also in Specimens E and J where the crack tips had nearly or completely run through on one side of the specimen.

For Specimens I and L, the slopes of the displacement curves were substantially larger than 1/2, thus indicating a decrease in the order of stress singularity due to multiple cracking. For Specimens E and J, the slopes of the log-log plot of the displacement curve were substantially less than 1/2. A plausible explanation for this deviation is that much of the load carried by the fractured side of the specimen was transferred to the remaining side and thus possibly increased the order of stress singularity and caused the crack to accelerate towards its terminal velocity.

The Moire fringe pattern of one specimen, Specimen D, was also scanned by a microdensitometer* for a more accurate determination of the locations of fractional fringes and hence an increased accuracy in y-displacement, v, determinations. This displacement distribution was then

* Joyce-Loebl Microdensitometer operated by Beckman & Whitley, Inc., San Carlos, California





graphically differentiated in the y-direction to obtain distribution of normal strains, $\varepsilon_{yy}$, which is shown in Figure 9a. This procedure is not only costly but strain determination through graphical differentiation is very time consuming and therefore a curve fitting procedure was developed to evaluate other experimental results.

The computer program used the method of least squares to determine the coefficients $C_{2m+1}$ of Equation 4 such that Equation 3b gave the best fit to the experimental data. It was determined that by selecting data points throughout the field of interest, the best representation of the strain fields was obtained. For these tests a maximum of 6 coefficients (i.e., $C_1$, $C_3$, $C_5$, $C_7$, $C_9$, $C_{11}$) was used to fit an average of 25 data points.

For the half crack length, a, in Equation 2, the distance between the center of the specimen and the crack tip in consideration was used. The reason for not using half of the actual total crack length is that the state of stresses further away from the running crack was still essentially that of the static stress distribution and that the end grips of the specimen had not rotated yet to account for the two uneven ligaments left at the crack section of the specimen.

The validity of the above method of determining strains through curve fitting a displacement curve was then evaluated by computing the normal strain, $\varepsilon_{yy}$, for Specimen D by this method. The results are shown in Figure 9b and are found to correlate closely with the results obtained by graphical differentiation as shown in Figure 9a.

Table II lists the polynomial coefficients and the dynamic stress intensity factors calculated by the computer for Specimens A, D and E.

From Table II it can be seen that as the number of coefficients used to fit the experimental data is increased from 2 to 6, the dynamic stress intensity factor converges toward a constant value. No more than 6 coefficients were used because smoothing of the experimental data was desired.

Also listed for comparison are the dynamic stress intensity factors determined graphically for these specimens. The difference between the dynamic stress intensity factors obtained by the computer and by graphical methods is primarily due to the fact that the graphical procedure is essentially an approximation of the stress intensity factor represented by Equation 6 and therefore will not account for the complex loading and boundary conditions imposed by a running crack in a finite width plate.

Using the Westergaard stress function determined by the above procedure, transient strain fields in the vicinity of the running crack tip were thus computed for Specimens A, D, E and L. These transient strain fields are shown in Figures 10 through 13. For this computation, a Poisson's ratio of $\nu = 0.38$ was used.

The dynamic stress intensity factors were also determined by use of Equation 6 for those specimens which were analyzed by the curve fitting procedure. This stress intensity factor requires the knowledge of the dynamic shear modulus which was not available. The dynamic modulus of elasticity of E = 495,000 psi as determined by Clark (15) for this particular type of material was used as an approximation. For specimens with 45° Moire grid orientation, the dynamic stress intensity factors were determined by the use of Equation 9. The log-log plot of the displacement versus distance was used to obtain the displacement at r = 0.1 inch for this calculation. These results are tabulated in Table III.

Also shown in Table III are the equivalent static stress intensity factors, $K_{se}$, for a total crack length of 2a, which is twice the distance between the center of the specimen and the running crack tip, and for an applied stress, σ, at fracture. Ratios of $K_d/K_{sc}$ and $K_d/K_{se}$ in this table show the stress magnifications caused by the running crack.

The crack velocities which would have yielded interesting correlation between the observed dynamic stress intensity factors were not determined in this series of studies.

Qualitative comparison of crack velocities was made by observing the texture of the fractured surface. An example of the range of the texture of such fractured surface can be seen in Figure 6. Previous investigations (14,16) showed that the fractured surface increases in roughness as the crack velocity approaches its terminal velocity prior to branching. The column, "fractured surface," in Table III is therefore shown to make a qualitative correlation between the crack velocities and the stress singularities through the texture of the fractured surface.

## CONCLUSIONS AND DISCUSSION

The results of this preliminary investigation show that the static characteristic of the $\frac{1}{\sqrt{r}}$ singularity holds in the vicinity of a running crack tip as predicted by theoretical analyses based on various mathematical models (5, 6, 7), provided the crack has not approached its terminal velocity and provided that branching and doubling of the crack do not occur.

The dynamic stress intensity factors at the instant of recording in these series were 2.3 to 5.5 times larger than the static fracture toughness of the material and are in agreement with the predictions made by Irwin (14). Also moderate correlation was obtained between the magnitude of this ratio and the texture of the cracked surface where the rougher cracked surfaces in general were accompanied by higher stress intensity factors.

For Specimen E, the crack ran through on one side thus leaving essentially a single edge-notched specimen which was the specimen configuration used by Wells and Post (1). As shown in Figure 12 the maximum shear strain





distribution, $\epsilon_{12}$, which corresponds to the isochromatics distribution through stress and strain optical coefficients, exhibits the tendency to bend forward towards the edge of the specimen as observed by Wells and Post.

On the other hand, for Specimen A where the crack tip had not progressed too far, the shape of the maximum shear stress distribution as shown in Figure 10 tends to lean backward towards the center of the specimen. This shape of the maximum shear strain distribution was predicted by Baker in his theoretical analysis (6).

For Specimens D and K, the maximum shear strain distributions as shown in Figures 11 and 13 extend straight up and are thus in qualitative agreement with the static theoretical results (17) for an infinite plate with a central crack.

## ACKNOWLEDGEMENT

The results obtained in this paper were obtained in a research project sponsored by the Office of Naval Research through Contract Nonr-447 (39) NR 064 478. The authors gratefully acknowledge the generous encouragement given them by Drs. H. Liebowitz and N. Perrone of ONR and by Dr. G. R. Irwin of NRL throughout the course of this investigation.

In addition, R. A. Selby was supported in part through a National Science Foundation Undergraduate Education in Science program. The authors also thank W. L. Engstrom, a NSF-UES participant, for assisting them in evaluating the test results.

## REFERENCES

1. Wells, A. A. and D. Post, "The Dynamic Stress Distribution Surrounding a Running Crack," Proc. of the Soc. for Exp. Stress Analysis, Vol. XVI, No. 1, 1958, pp. 69-92.

2. Irwin, G. R., "Discussion" of the above reference, ibid., pp. 93-96.

3. Rolfe, S. T. and W. J. Hall, "Strain Field Associated with Brittle-fracture Propagation in Wide Steel Plates," Experimental Mechanics, Vol. 1, No. 9, September 1961, pp. 113-119.

4. Cargill, J. M., "Strain Field Set Up on a Plate Surface by a Running Brittle Crack," J. of Mech. Engg. Sciences, Vol. 5, No. 1, 1963, pp. 28-37.

5. Yoffe, E. H., "The Moving Griffith Crack," Phil. Mag., Series 7, Vol. 42, 1951, pp. 739-750.

6. Baker, B. R., "Dynamic Stresses Created by a Moving Crack," J. of Applied Mechanics, Trans. of ASME, Vol. 29, Series E, No. 3, September 1962, pp. 449-458.

7. Craggs, J. W., "On the Propagation of a Crack in an Elastic-Brittle Material," J. of the Mechanics and Physics of Solids, Vol. 8, 1960, pp. 66-75.

8. Morse, S., A. J. Durelli, and C. A. Sciammarella, "Geometry of Moire Fringes in Strain Analysis," J. of Engg. Mechanics Div., Proc. of ASCE, August 1960, pp. 105-126.

9. Durelli, A. J., C. A. Sciammarella, and V. J. Parks, "Interpretation of Moire Patterns," J. of Engg. Mechanics Div., Proc. of ASCE, April 1963.

10. Riley, W. F. and A. J. Durelli, "Application of Moire Methods to Determination of Transient Stress and Strain Distributions," J. of Applied Mechanics, Trans. of ASME, Vol. 29, Series E, No. 1, March 1962, pp. 23-29.

11. Sciammarella, C. A., B. E. Ross, and D. Sturgeon, "Thermal Stresses at High Temperatures in Stainless Steel Rings by the Moire Method," Technical Report, Dept. of Engg. Science and Mechanics, University of Florida, December 1964.

12. Westergaard, H. M., "Bearing Pressures and Cracks," J. of Applied Mechanics, Trans. of ASME, June 1939.

13. Irwin, G. R., "Fracture," Handbuch der Physik, Vol. 6, Elastizitat und Plastizitat, Springer (Berlin), 1958, pp. 551-590.

14. Clark, A. B. J. and G. R. Irwin, "Crack Propagation Behavior," to be published in the J. of Experimental Mechanics.

15. Clark, A. B. J. and R. J. Sanford, "A Comparison of Static and Dynamic Properties of Photoelastic Materials," J. of Experimental Mechanics, Vol. 3, No. 9, June 1963, pp.148-151.

16. Krafft, J. M. and G. R. Irwin, "Crack Velocity Considerations," Proceedings of the ASTM Symposium on Fracture Toughness Testing and Its Application, 1965.

17. Sneddon, I. N., "The Distribution of Stress in the Neighborhood of a Crack in an Elastic Solid, "Proc. of Roy. Soc., A, Vol. 187, 1945.





TABLE I

SPECIMEN SPECIFICATIONS AND STATIC FRACTURE DATA

| Specimen | Moire Grid Orientation | Initial Mismatch in Moire Fringes | Initial Crack Length 2a | Static Fracture Toughness $K_{sc}$ psi $\sqrt{in.}$ |
|---|---|---|---|---|
| A | 0° and 90° | Approx. 8 fringes/in. | ---- | ----- |
| B | " | " | ---- | ----- |
| C | " | " | 0.66 | 293 |
| D | " | " | 0.26 | 327 |
| E | " | " | 0.75 | 308 |
| F | 45° | " | 0.35* | 348 |
| G | " | " | 0.52 | 293 |
| H | " | " | 0.40* | 356 |
| I | 0° and 90° | " | 0.50 | 316 |
| J | 45° | " | 0.73 | 286 |
| K | 0° and 90° | Approx. 35 fringes/in. | 0.28 | 314 |
| L | " | " | 0.30* | 383 |
| Average | | | | 305** |

* Blunt Crack Front

** Average of 7 specimens with sharp initial crack

Specimen Material

Araldite 502 resin with 10 pphr HN 951.

Specimen Material Properties

| | |
|---|---|
| Static Modulus of Elasticity | E = 375,000 psi |
| Static Poisson ratio | $\nu$ = 0.38 |
| Dynamic Modulus of Elasticity | E = 495,000 psi* |

* From Reference 15

TABLE II

COEFFICIENTS OF WESTERGAARD'S STRESS FUNCTION AND DYNAMIC STRESS INTENSITY FACTORS

| SPECIMEN | Coefficients $C_1$ | $C_3$ | $C_5$ | $C_7$ | $C_9$ | $C_{11}$ | Dynamic Stress Intensity Factor Calculated psi $\sqrt{in.}$ | Graphical psi $\sqrt{in.}$ |
|---|---|---|---|---|---|---|---|---|
| A | 0.0017930 | -0.0000326 | | | | | | |
| | 0.0037493 | -0.0010430 | 0.0000968 | | | | 690 | |
| | 0.0044898 | -0.0011732 | -0.0000121 | 0.0000197 | | | 682 | |
| | 0.0030794 | 0.0000804 | -0.0004407 | 0.0001018 | -0.0000077 | | 686 | |
| | -0.0010267 | 0.0076308 | -0.0049267 | 0.0013380 | -0.0001931 | 0.0000133 | 703 | |
| | | | | | | | 716 | 741 |
| D | 0.0028639 | 0.0008334 | | | | | | |
| | 0.0037093 | 0.0002551 | 0.0000719 | | | | 1633 | |
| | 0.0036059 | 0.0000169 | 0.0002335 | -0.0000212 | | | 1641 | |
| | 0.0046963 | -0.0011877 | 0.0006992 | -0.0001136 | 0.0000085 | | 1595 | |
| | 0.0047149 | -0.0012352 | 0.0007325 | -0.0001236 | 0.0000100 | -0.0000001 | 1584 | |
| | | | | | | | 1583 | 1480 |
| E | 0.0038994 | -0.0006098 | | | | | | |
| | 0.0052453 | -0.0014737 | 0.0000552 | | | | 1046 | |
| | 0.0064271 | -0.0017545 | -0.0004348 | 0.0001359 | | | 1087 | |
| | 0.0064659 | -0.0018069 | -0.0004078 | 0.0001278 | 0.0000012 | | 1107 | |
| | 0.0062074 | -0.0010221 | -0.0011595 | 0.0004571 | -0.0000767 | 0.0000088 | 1106 | |
| | | | | | | | 1108 | 1270 |





TABLE III

DYNAMIC FRACTURE DATA

| Specimen | Slope of displacement curve on a log-log plot | Half Crack Length a* at the Instant of Recording in. | Equivalent Static Stress Intensity Factor $K_{se}$ psi $\sqrt{in.}$ | Dynamic Stress Intensity Factor** $K_d$ psi $\sqrt{in.}$ | $\frac{K_d}{K_{sc}}$ (av.) | $\frac{K_d}{K_{se}}$ (equiv.) | Texture of Fractured Surface at the Instant of Recording | Remarks |
|---|---|---|---|---|---|---|---|---|
| A | 1/2.11 | 1.62 | --- | 716*** | 2.35 | --- | | |
| B | 1/1.96 | 0.98 | --- | 710 | 2.26 | --- | | |
| C | 1/1.95 | 1.07 | 527 | 811 | 2.66 | 1.54 | Smooth | |
| D | 1/1.77 | 1.36 | 1058 | 1480*** | 4.53 | 1.40 | Slightly Rough | |
| E | 2.43 | 1.26 | 564 | 1108*** | 3.60 | 1.96 | Smooth | Crack ran through on one end |
| F | 1/1.95 | 1.57 | 1042 | 1136 | 3.75 | 1.09 | Rough | |
| G | 1/1.88 | 1.22 | 634 | 797 | 2.61 | 1.26 | Slightly Rough | Measurements at two crack tips |
| | 1/2.00 | 1.54 | 713 | 996 | 3.27 | 1.40 | " " | |
| H | 1/2.04 | 1.18 | 863 | 1530 | 5.01 | 1.77 | Very Rough | |
| | 1/2.17 | 1.47 | 966 | 1677 | 5.47 | 1.74 | " " | |
| I | 1/16-1/1.3 | 0.62 | --- | ---- | -- | -- | Jagged | Two parallel cracks at one end |
| J | 1/2.48 | 1.72 | 621 | 1038 | 3.41 | 1.67 | Smooth | Crack tip very close to the edge |
| K | 1/1.93 | 1.03 | 851 | 1684*** | 5.52 | 1.98 | Slightly Rough | |
| L | ≈1/1.4 | 1.28 | --- | ---- | -- | -- | Jagged | Crack branched on both sides |
| | --- | 1.66 | --- | ---- | -- | -- | " | |

* Note that half width of the specimen is 2.00 in. Half crack length is measured from the center of the specimen.

** Determined graphically unless stated otherwise.

*** Determined by fitting Westergaard's stress function, Z.

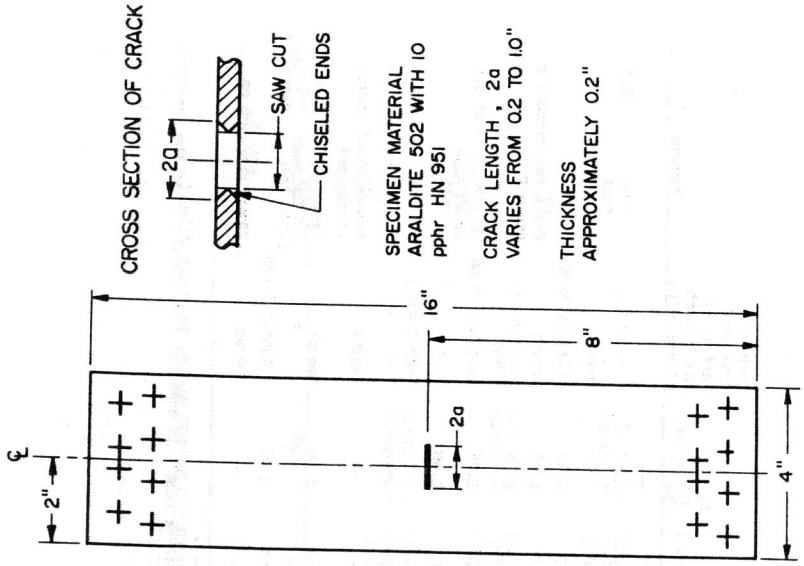


FIGURE 2. CENTRALLY NOTCHED SPECIMEN

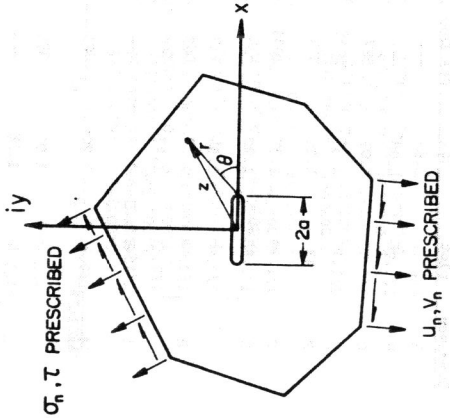


FIGURE 1. FINITE PLATE WITH A CRACK SUBJECTED TO ARBITRARY LOADING.





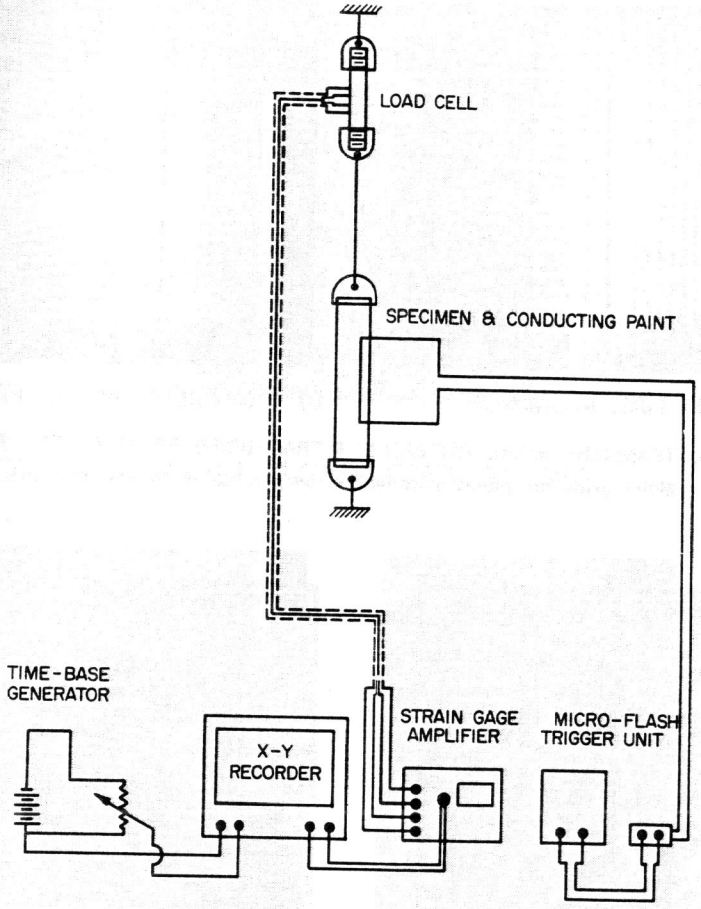


FIGURE 3. INSTRUMENTATION DIAGRAM

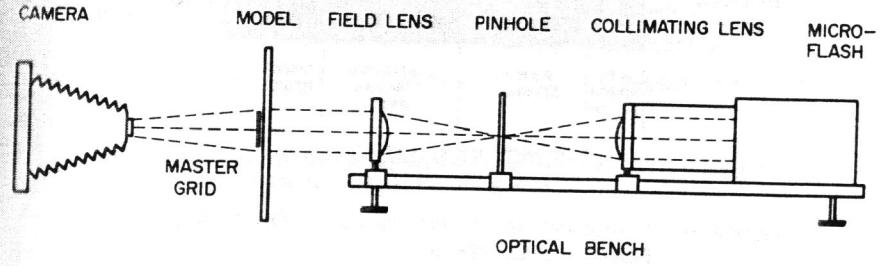


FIGURE 4. HIGH SPEED PHOTOGRAPHIC SYSTEM

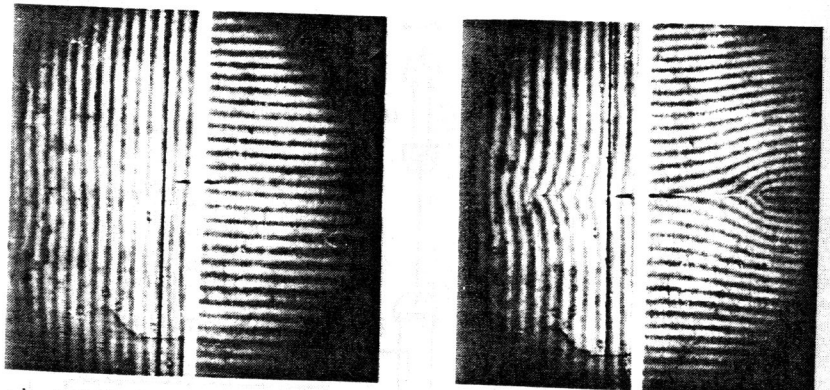

a) INITIAL MISMATCH b) TRANSIENT MOIRE PATTERN

FIGURE 5. TRANSIENT MOIRE PATTERN IN A FRACTURING EPOXY PLATE, SPECIMEN D
Moire grids are placed parallel and perpendicular to specimen axis.

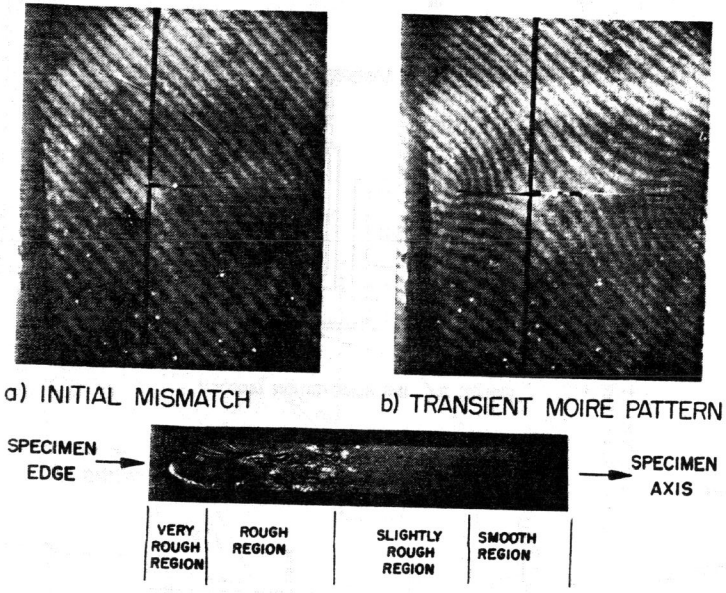


a) INITIAL MISMATCH b) TRANSIENT MOIRE PATTERN

c) FRACTURED SURFACE

FIGURE 6. TRANSIENT MOIRE PATTERN IN A FRACTURING EPOXY PLATE SPECIMEN H
Moire grids are placed 45° to the specimen axis





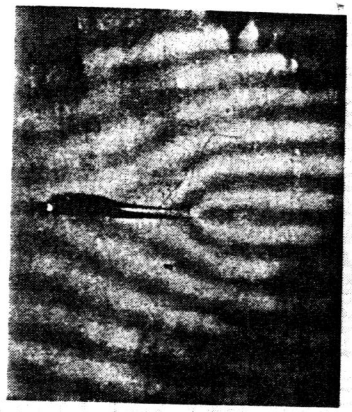

a) DOUBLE RUNNING CRACK SPECIMEN I

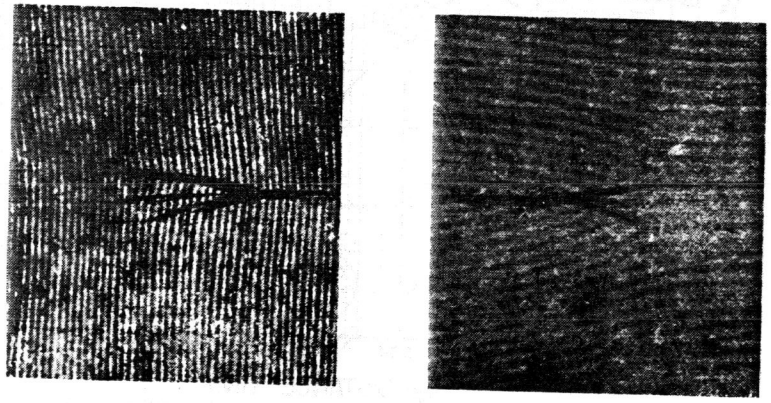

b) BRANCHING CRACKS, SPECIMEN L
Moire patterns are reversed due to compression mismatch

FIGURE 7. TRANSIENT MOIRE PATTERNS IN THE VICINITY OF MULTIPLE CRACKS IN FRACTURING EPOXY PLATE.

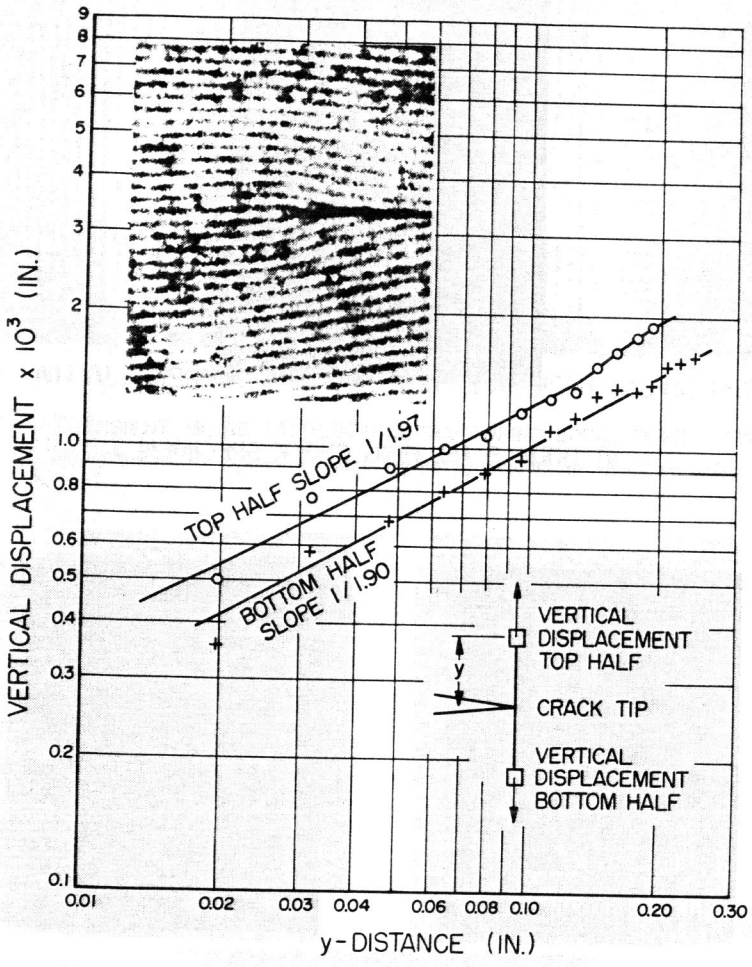


FIGURE 8. VERTICAL DISPLACEMENT PLOT IN THE VICINITY OF A RUNNING CRACK TIP — SPECIMEN K.





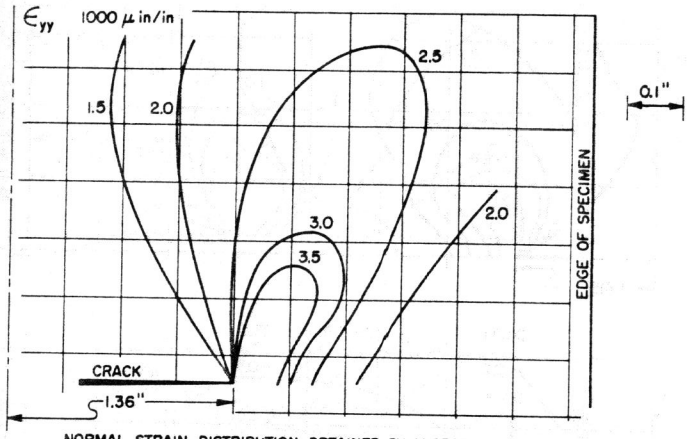


NORMAL STRAIN DISTRIBUTION OBTAINED BY MICRODENSITY TRACINGS

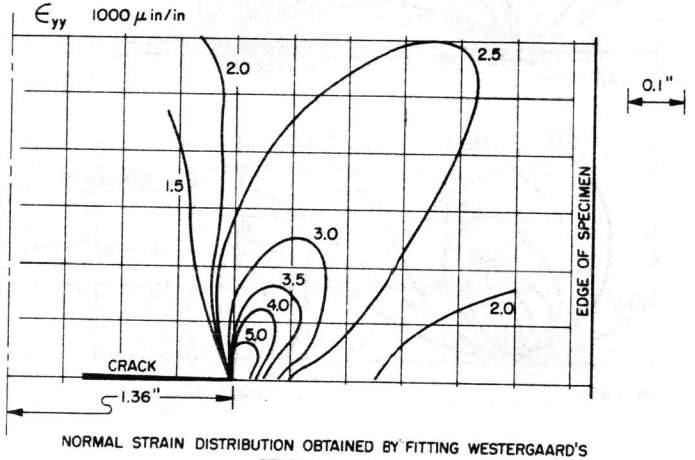


NORMAL STRAIN DISTRIBUTION OBTAINED BY FITTING WESTERGAARD'S STRESS FUNCTION

FIGURE 9. COMPARISON OF NORMAL STRAIN DISTRIBUTIONS OBTAINED BY MICRODENSITY TRACINGS AND FITTING WESTERGAARD'S STRESS FUNCTION SPECIMEN D

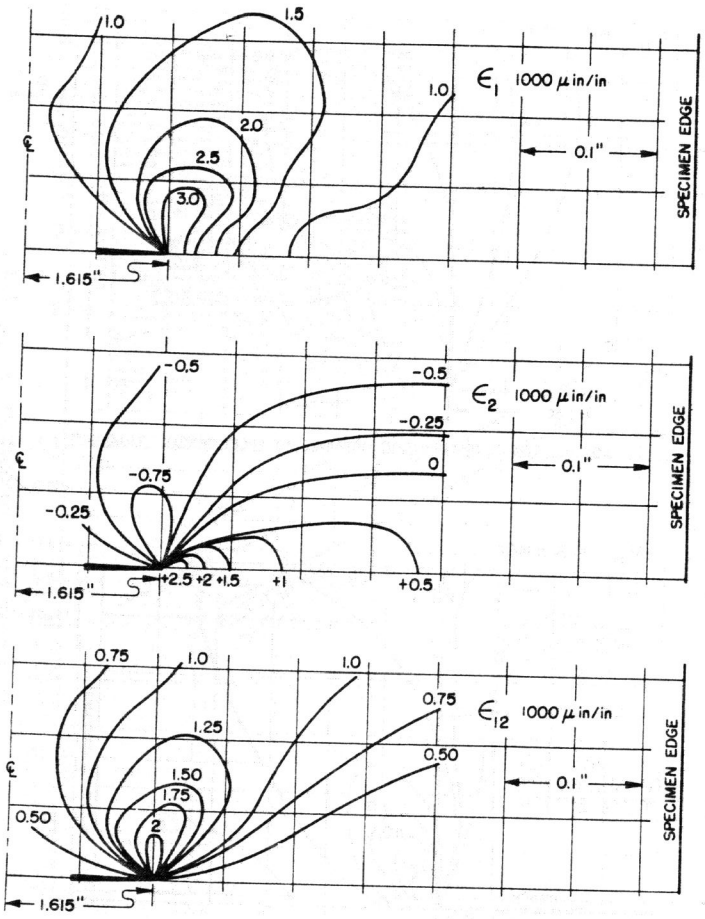


FIGURE 10. PRINCIPAL STRAIN AND MAXIMUM SHEAR STRAIN DISTRIBUTIONS IN THE VICINITY OF A RUNNING CRACK SPECIMEN A





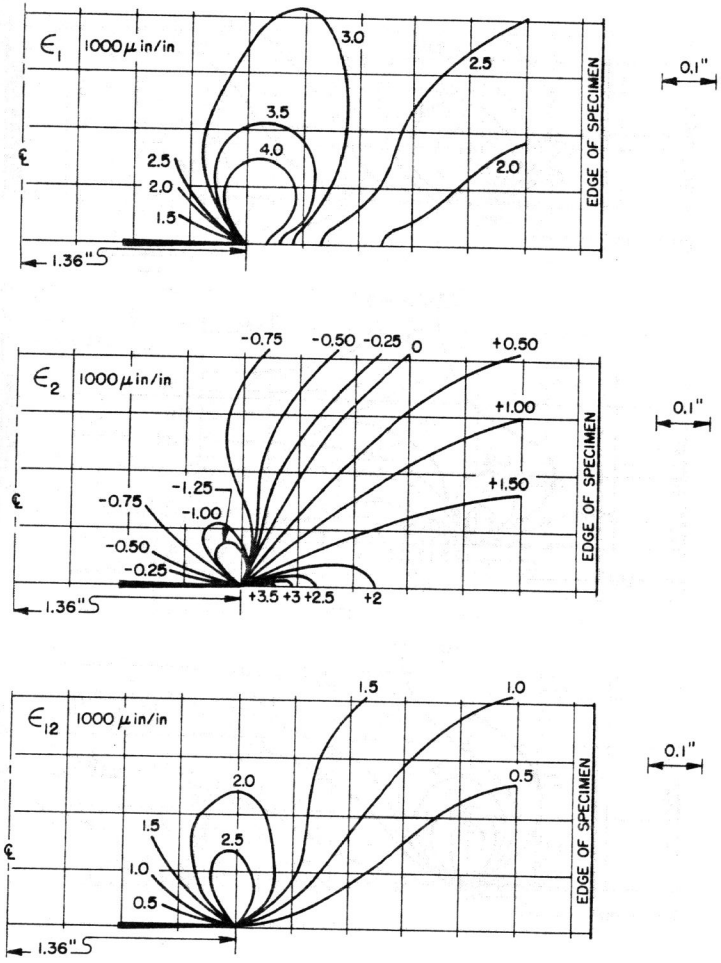


FIGURE 11. PRINCIPAL STRAIN AND MAXIMUM SHEAR STRAIN DISTRIBUTIONS IN THE VICINITY OF A RUNNING CRACK SPECIMEN D

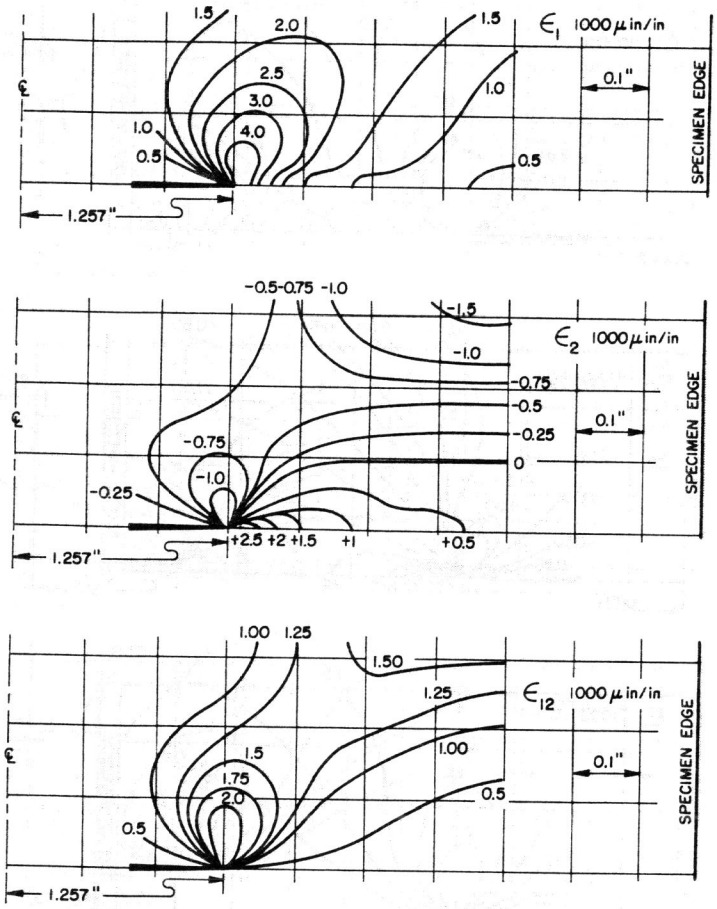


FIGURE 12. PRINCIPAL STRAIN AND MAXIMUM SHEAR STRAIN DISTRIBUTIONS IN THE VICINITY OF A RUNNING CRACK SPECIMEN E





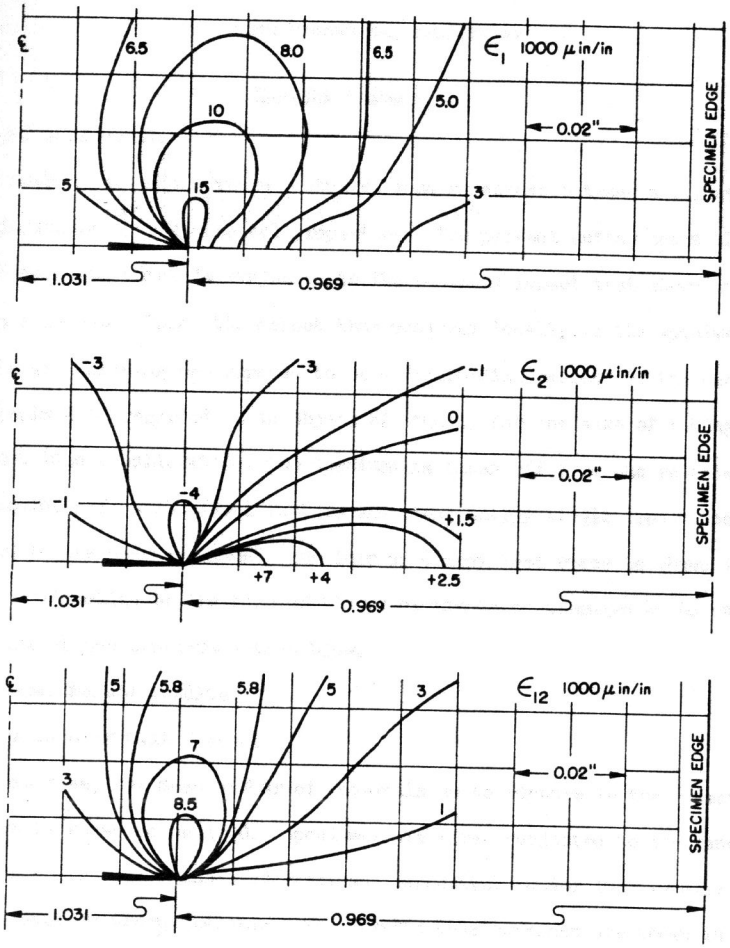


FIGURE 13. PRINCIPAL STRAIN AND MAXIMUM SHEAR STRAIN DISTRIBUTIONS IN THE VICINITY OF A RUNNING CRACK SPECIMEN K